Flexible Meta-Signal Tracking: Architecture Robustness in Challenging PNT Scenarios

Flexible Metasignal Tracking: Architecture Robustness in Challenging PNT Scenarios

ANDREA NARDIN, Graduate Student Member, IEEE
FABIO DOVIS, Member, IEEE
Politecnico di Torino, Turin, Italy

FRANCESCA ZANIER
FLOOR MELMAN
European Space Agency, Noordwijk, The Netherlands

The idea of multichannel tracking is generally found in the global navigation satellite system (GNSS) literature with a wideband approach. We further developed the concept to separately process two narrowband channels that are later combined in a dedicated delay-locked loop in a virtual wideband fashion. To suit the prospect evolution of positioning, navigation, and timing (PNT) technologies and GNSSs, we generalized the so-called metasignal construction to the combination of components transmitted over the same bandwidth, thus expanding the range of candidate multichannel components and fostering efficient bandwidth exploitation and increased resiliency to harsh Doppler. These improvements are sustained by additional complexity at the receiver, whose robustness must be carefully assessed. The resulting architecture performance in the presence of multipath and tracking noise is, therefore, characterized under the challenging conditions of modern GNSSs, focusing on a low Earth orbit PNT scenario. The technique can successfully bear the representative Doppler profiles and C/N_0 levels of the addressed scenarios achieving a large estimation noise reduction, even under challenging multipath conditions.

Manuscript received 1 August 2023; revised 1 December 2023; accepted 21 January 2024. Date of publication 29 January 2024; date of current version 11 June 2024.

DOI. No. 10.1109/TAES.2024.3359594

Refereeing of this contribution was handled by O. Osechas.

This work was supported by European Space Agency (ESA) within the framework of the activity *INNovative User receiver processing and ENhanced signals in gnss DOmain* (INNUENDO).

Authors' addresses: Andrea Nardin and Fabio Dovis are with Politecnico di Torino, 10124 Turin, Italy, E-mail: (andrea.nardin@polito.it; fabio.dovis@polito.it); Francesca Zanier and Floor Melman are with European Space Agency, 2201 Noordwijk, The Netherlands (e-mail: francesca.zanier@esa.int; floor.melman@esa.int). *(Corresponding author: Andrea Nardin.)*

I. INTRODUCTION

In addition to Earth-based navigation, positioning, navigation, and timing (PNT) services are already exploited in a plethora of applications [1]. Among these are precision agriculture [2], vehicle and interpersonal ranging [3], [4], [5], communication networks [6], or space applications [7], [8], [9], to name a few. However, as the range of applications expands, providing an adequate PNT service is becoming more challenging and, nevertheless, an increasing number of current and envisioned applications demands a precise and reliable PNT system [1]. In the framework of global navigation satellite systems (GNSSs) and more generally radio navigation systems (RNSs), several approaches are exploited or have been proposed to fulfill this requirement, either on the signal design side [10], [11] or through innovative processing architectures [12], [13], [14].

Among these solutions, the availability of synchronous channels can be exploited to increase the precision and the robustness of the position estimate through a *multichannel (MC)* approach, implemented within the processing chain of a receiver. A satellite constellation that offers multiple PNT services or data/pilot channels may, indeed, transmit more than one signal component per satellite vehicle and these components are generally synchronous to some extent, especially if they undergo the same transmission chain (frequency up-converter, amplifier chain, and antenna) [15], [16] when multiplexed together. Multiple channels availability is already a reality for GNSSs [17] and some degree of service multiplicity will be likely accommodated also by the next generation of alternative and complementary PNT technologies [14], [18], [19], [20], [21], [22], [23].

The coherency among these signals can be exploited to improve the quality of the information that is going to be extracted from them. Referring to a classical GNSS receiver architecture [24], the coherent transmission of direct sequence spread spectrum (DSSS) signal components allows coherent MC *tracking*, thus merging the information content of signals at an early stage of the signal processing chain [15], [16], [25], [26], [27], [28]. As a result, the MC approach efficiently exploits, at a tracking level, the availability of multiple signal components to address more accurate and precise navigation solutions while improving robustness to common impairments such as multipath (MP) and interference [29]. A single signal composed of synchronous GNSS channels received at different frequencies has been regarded as *metasignal* [30], [31], [32], [33]. In recent years, the use of metasignals processed as a single wideband signal has been investigated as a promising approach to effectively take advantage of multiple channels availability and extract high-quality measurements to improve positioning accuracy [32], [33], [34], [35], [36], [37].

Metasignals, however, as well as split-spectrum modulations, are generally characterized by a multipeaked autocorrelation function (ACF) [38]. A characteristic that might lead to false locking and biased measurements, especially when MP is present. Such an aspect must be, therefore, addressed in working implementations, adopting

a *peak ambiguity resolution* strategy. Nonetheless, an efficient exploitation of the many available signals is limited to the combination of those signal components that are transmitted over different frequencies. Indeed, in modern GNSSs, signal components might be transmitted over the same bandwidth, carried by in-phase and quadrature carriers (e.g., Galileo E5a-I and E5a-Q) or orthogonal pseudo-random codes (e.g., E1B and E1C) [39]. In addition, the construction of such wideband metasignals might not suit the prospect evolutions of PNT technologies and GNSSs, such as low Earth orbit (LEO) PNT systems [14], [19], [40], [41], where payload is designed for rapid reconfiguration and signal components might be sharing the same bandwidth [41]. Nonetheless, signals transmitted by LEO satellites are received on Earth after experiencing severe Doppler shifts, a major cause of distortion for wideband signals.

To overcome these limitations, we generalize the metasignal construction to the combination of signal components transmitted over the same bandwidth, thus expanding the MC approach to other forms of signal orthogonality, other than frequency separation [14], [22], [42]. This flexible approach can be adapted to dynamic payloads and signals configurations. Moreover, it fosters efficient bandwidth exploitation, resulting in the use of narrower bandwidths and an increased resiliency to harsh Doppler [14] but its robustness in challenging scenarios must be carefully investigated. Indeed, the performance improvements brought in by this approach are generally sustained by an additional complexity at the receiver side, which, if not carefully addressed, can easily undermine its robustness, especially in harsh environments and modern GNSS scenarios. An implementation of this concept was preliminary investigated in [14], [22], and [42] and dubbed *virtual wideband (VWB) tracking*. This original architecture has been improved to attain a more robust ambiguity resolution and better cope with MP-induced biases. Nevertheless, a comprehensive characterization of its performance in modern challenging scenarios has never been addressed.

The objective of this work is, therefore, twofold. On the one hand, we want to deeply characterize this flexible metasignal architecture in a LEO PNT context. On the other, we want to test the implementation's performance, focusing on its robustness and stressing the conditions that might lead to false locking. The rest of the article is organized as follows. In Section II, a description of the proposed implementation is followed by the ambiguity resolution strategy adopted. The behavior of the proposed method in challenging conditions is then assessed in a relevant LEO PNT scenario. A detailed performance analysis is provided, addressing, in particular, (i) the MP impact and the associated risk of false locking, and (ii) the robustness of the architecture to tracking noise. The study logic behind experimental campaigns (i)–(ii) is outlined in Section III while the resulting outcomes are provided in Section IV. Finally, Section V concludes this article.

II. VWB METASIGNAL AND TWO-STEP PEAK DISCRIMINATION

A. Metasignal Rationale

The metasignal concept introduced in [30] is based on the well-known Cramér–Rao bound (CRB) that limits the minimum achievable propagation time estimator variance σ_τ^2 such that [43]

$$\sigma_\tau^2 \geq \frac{1}{8\pi^2\eta\beta^2} = \frac{1}{8\pi^2\frac{C}{N_0}T\beta^2} \tag{1}$$

where

$$\beta^2 \triangleq \frac{\int_{-\infty}^{+\infty} f^2|X(f)|^2}{\int_{-\infty}^{+\infty} |X(f))|^2} \tag{2}$$

is the square of the so-called Gabor bandwidth (GB). In the equation, the dependence on the signal-to-noise ratio (SNR) $\eta = \frac{C}{N_0}T$ is highlighted [38], [44] where T is the observation time and $\frac{C}{N_0}$ is the *carrier-to-noise-density ratio (C/N$_0$)*. The GB in (2) depends on the spectrum $X(f)$, which is the Fourier transform of the baseband noiseless observed signal $x(t)$ [43], [44].

It is clear that the CRB of the propagation time estimator can be reduced by increasing the GB. The net effect is to achieve, in turn, an improved position estimation in those RNSs based on time of arrival (TOA). In the GNSS literature, in the past years, several solutions have been proposed to achieve a larger GB. The methods differ from the way in which the increase of the GB is obtained. The straightforward, well-known, way, is the use of wider bandwidth signals, thus occupying a wider range of the frequency axis. However, in recent years, it has been proposed to achieve better resolution by processing "all together" several, narrowband, GNSS channels, received over different carrier frequencies. This approach has been referred, in general, as the use of GNSS *metasignals*.

B. Generalized Metasignal Model

Let us consider a set of N signals $s_i(t)$ with $i = 1, \ldots, N$, merged together into the signal $x(t)$, processed by a TOA estimator. According to (1), it is desirable to have a signal $x(t)$ with a large GB. Under an MC approach, this can be obtained if the processed channel components are spread over the spectrum of $x(t)$ such that

$$x(t) = \sum_{i=1}^{N} s_i(t)e^{j2\pi f_i t} \tag{3}$$

has a large part of its energy located at the spectrum edges. An approximation of (3) can be easily obtained as a complex baseband of a received radio frequency (RF) signal if the relative frequency separation among the signal components within $x(t)$ matches the frequency separation among the components in the transmitted signal at RF. This MC composite signal, processed as a single signal, is known as *metasignal* (here generalized to N signals). Nevertheless,

if each signal $s_i(t)$ can be separately processed by a receiver, a composite signal whose complex baseband has the form in (3) can be effectively obtained within the receiver processing chain by modulating each carrier at f_i with the ith signal component $s_i(t)$. The net result is still a large GB signal that enters a TOA estimator. It is worth stressing that this approach can work as long as signal components can be independently processed, i.e., as they are orthogonal signals. As a result, this generalized metasignal construction can be extended also to components transmitted over the same bandwidth, e.g., by means of in-phase and quadrature carriers or orthogonal spreading codes.

Commonplace TOA estimators are implemented through correlators. The correlation properties of a signal $x(t)$ are well-described by its ACF, defined as

$$R_{xx}(\tau) = \int_{-\infty}^{+\infty} x(t+\tau)x^*(t)\,\mathrm{d}t. \tag{4}$$

A signal with a large GB shows a narrow main peak, a property that is, indeed, related to a good code-tracking performance, i.e., to an accurate TOA estimation [45]. Nevertheless, it can be proved [46], that the ACF of a metasignal, as defined in (3), can be approximated by the sum of the ACF of its component signals modulating complex exponentials [31]. In other words

$$R_{xx}(\tau) \approx \sum_{i=1}^{N} R_{x_i x_i}(\tau) = \sum_{i=1}^{N} R_{s_i s_i}(\tau) e^{j2\pi f_i \tau} \tag{5}$$

where $x_i(t) = s_i(t)e^{j2\pi f_i t}$. Note that the approximation in (5) becomes an equality when the signals $s_i(t)$ are confined to disjoint bandwidths.

C. VWB Architecture

The generalization of the metasignal concept to other forms of signal orthogonality motivated the development of a tracking architecture that can, on the one hand, process an MC signal whose complex baseband representation has the form in (3) and, on the other, drive the generation of each f_i carrier in a closed-loop fashion. The block scheme in Fig. 1 illustrates such architecture.

Without loss of generalization, the scheme describes a tracking stage for $N = 2$ channels. Two received intermediate frequency (IF) signals, $y_{1,\mathrm{IF}}(t)$ and $y_{2,\mathrm{IF}}(t)$, undergo the two codependent loops for carrier and code wipe-off, typical of a GNSS receiver's tracking stage [17]. Then, before entering in an MC delay-locked loop (DLL), a local numerically-controlled oscillator (NCO), driven by the DLL, is used to obtain the desired frequency separation f_m between the processed components.

Inside the DLL (see Fig. 2), the two channels are combined at a postcorrelation level, exploiting the property in (5) and, thus, merging the correlators outputs instead of the metasignal components. In the proposed scheme, a classical *early-late* (E-L) architecture is used [24]. It is worth highlighting the introduction of a single-loop filter and a single-code NCO in the MC DLL. These originally separated blocks [22], [42] are now merged to reduce

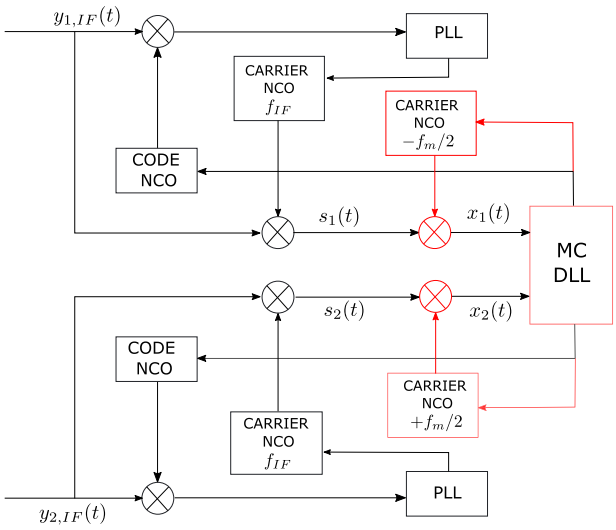

Fig. 1. VWB tracking implementation (second step). Distinctive blocks are highlighted in red.

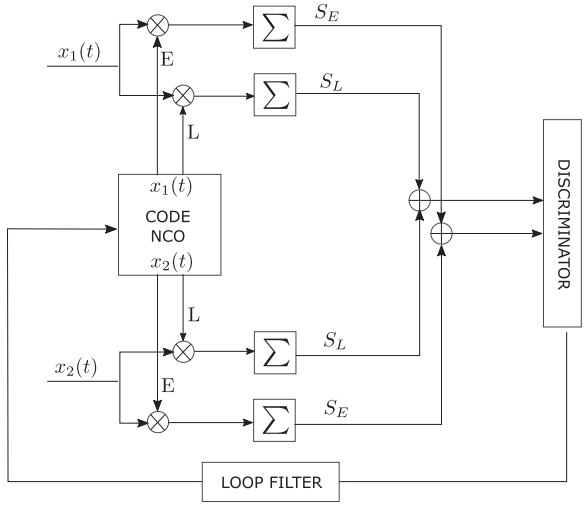

Fig. 2. MC DLL implementation.

the independence of the interconnected loops of the two channels, thus providing a more robust estimation. The discriminator behavior can be described by the so-called *S-curve*, a nominal characteristic function that depends on signals' ACF and the discriminator function and relates the discriminator output with the local replicas shift in the correlators [17].

D. Ambiguity Resolution and False Locking

A major problem with metasignals is that they exhibit a multipeaked ACF (see Fig. 3 as an example with two signal components). Therefore, at low SNR, side peaks can rise above the main peak leading to false locking and, in turn, to a biased TOA estimation, a well-known problem for narrowband signals [47], [48]. This means that, if we can cope with the ambiguity, it is possible to leverage the increased sharpness to reduce the correlator E-L spacing while keeping the same gap between Prompt (P) and Early

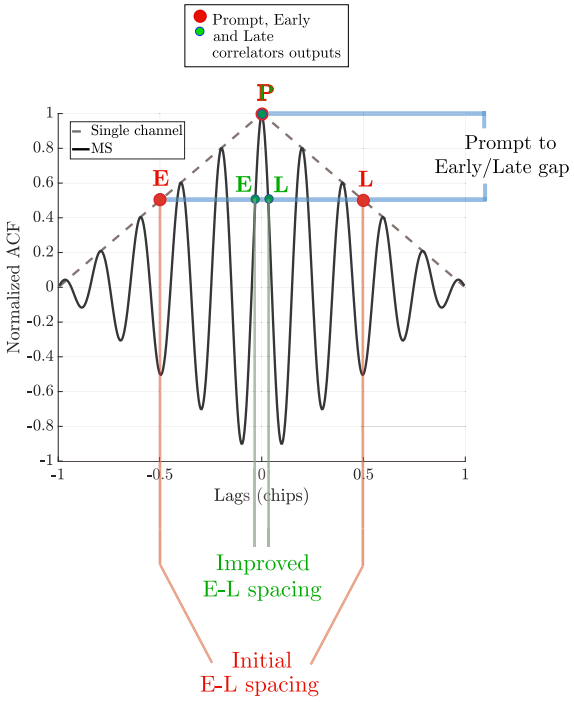

Fig. 3. ACF of a single BPSK(1) signal and a metasignal made by two BPSK(1) channels.

(E) or Late (L) correlator outputs (see Fig. 3). As a consequence, we can tolerate the same amount of noise (thanks to the gap) while obtaining a reduced code tracking jitter (thanks to the E-L spacing reduction) [24].

The number of peaks and, therefore, the severeness of the ambiguity depends on the frequency separation between the combined channels. Hence, a working tracking stage implementation should overcome the peak ambiguity through suitable techniques. This can be achieved, for instance, by resorting to ambiguity resolution methods developed for high-order binary offset carrier modulations [49], [50] or by implementing a *two-step* processing of the composite signal, where, during an initial step, each signal component is tracked independently allowing the correlators to align unambiguously on the main peak [31] (see [46], for a nonexhaustive discussion on ambiguity resolution methods for metasignals). Indeed, the inherent flexibility of the MC approach allows us to seamlessly move from a single channel (SC) step, where a plain tracking stage is used, to an MC step, when the architecture in Fig. 1 is adopted. After an initial SC tracking, the MC processing is triggered based on a locking condition, which might be based on a phase lock indicator (PLI) [51], defined as

$$\mathrm{PLI} = \frac{I_P^2 - Q_P^2}{I_P^2 + Q_P^2} \tag{6}$$

where I_P and Q_P are, respectively, the in-phase and quadrature phase prompt correlator outputs [17], computed at each tracking loop iteration. The MC stage is then enabled when the PLI is above a given threshold, defined as a receiver parameter. It is worth remarking that the use of a lock

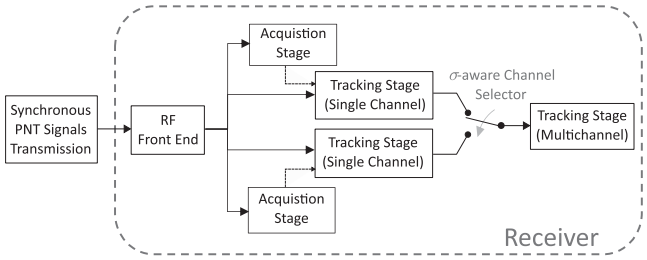

Fig. 4. End-to-end system architecture using a two-step ambiguity resolution method. Example with $N = 2$ channels.

detector during the SC step is an essential part of the proposed architecture, as it enables a profitable MC stage. Its observation in subsequent stages is not vital to a working implementation but could be exploited as a performance indicator.

A high-level overview of these sequential stages is provided by Fig. 4.

Notice that a *σ-aware channel selector* has been employed to obtain a more robust transition between the SC and MC step. This block allows us to select which of the N SC tracking output flows will be used to initialize the MC code NCO and DLL loop filter blocks. This selection is based on the statistical characteristics of the filtered discriminator output, as estimated by each SC tracking stage. In particular, the channel that exhibits the lower variance, estimated over a window of accumulated observations, is selected to initialize the subsequent MC stage. The selector has been introduced with respect to previous designs [22], [42] to prioritize the channel characterized by a potentially more robust estimation while taking advantage of the channel diversity.

III. STUDY LOGIC

A detailed characterization of the architecture was pursued through an experimental campaign, carried out with the scope of characterizing the implementation's robustness under challenging conditions. The results of this experimental campaign are provided in Section IV. In particular, we investigated the following:

1) the technique's behavior under unfavorable MP conditions associated with a high risk of false locking (see Section IV-A);
2) the technique's robustness to larger DLL noise bandwidths, exploring its behavior with respect to the amount of noise that can be tolerated in the tracking loop (see Section IV-B).

The performance analysis was performed with respect to a target LEO PNT scenario, assuming transmitted signal waveforms that are known to the receiver. The investigation of a signals-of-opportunity approach of the proposed method is out of the scope of this work [52]. To process realistic LEO PNT signals, a PNT receiver must be fed with signals characterized by Doppler profiles, which are consistent with the reference LEO constellation. A constellation

TABLE I
Common Configuration for the Experiments

Domain	Parameter	Value
Orbital Parameters	Inclination	51.9°
	Altitude	1200 km
Transmitter parameters	Modulation	BPSK(1)
	DSSS code length	1023
	Data rate	50 b/s
	CDMA spread	20460 chips/b
	Bandwidth	2.046 MHz
	Carrier frequency	1062 MHz (L band)
	Edge of coverage	30°
Atmospheric impairments	Cloud and Fog model	ITU-R P840-6
	Tropospheric scintillation	ITU-R P618-12
	Ionospheric fading	ITU-R P531-13
User conditions	User Location	Noordwijk (52.24°,4.45°)
Signal generator	Sampling frequency	25 MHz
	IF	0 Hz
	Code delay	0.5 ms
	Binary signal type	int8
	Quantization bits	7
	Antenna gain	0 dBi
Receiver configuration	PLL order	3
	SC E-L spacing	1 chip
	MC E-L spacing	0.025 chip
	PLI threshold	0.8
	Virtual frequency separation (f_m)	18.414 MHz
	Coherent integration time	1 ms
	DLL noise bandwidth	20 Hz
	PLL noise bandwidth	40 Hz

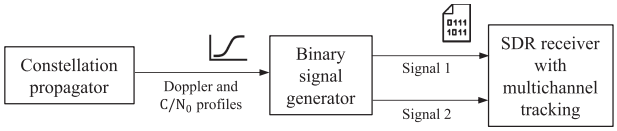

Fig. 5. Simulation blocks.

propagator tool (AGI STK) was used to simulate the LEO satellites and to model the communication channel. After selecting a user location on Earth, we were able to extract the frequency shift experienced by the receiver on Earth during the satellite passage due to the Doppler effect. Despite the potentially higher received power that should characterize LEO PNT frameworks [20], a more conservative choice of C/N_0 levels allows us to stress the implementation robustness while targeting power levels closer to the usual medium Earth orbit GNSS range. C/N_0 and the Doppler profile were used to feed a binary signal generator. The signal generator outputs two signals consistent with the Doppler profile and the C/N_0 level provided. These signals are then combined in an MC fashion within the tracking stage of a software receiver. An overview of the simulation blocks is provided in Fig. 5.

A general view of the parameters configuration of the test campaigns is reported in Table I. The values in the domain of "orbital parameters," "transmitter parameters," "atmospheric impairments," and "user conditions" were used to model the LEO constellation simulator block in Fig. 5. An altitude of 1200 km was set to target a realistic LEO PNT scenario, inspired by OneWeb [53] and Starlink [54] constellations. The values reported in the "signal generator" domain were used to set up the signal simulator for the generation of binary samples and those relative to "receiver configuration" were set to properly tune the software receiver to process the generated digital signals. The signals involved in the simulations are BPSK(1) signals with the same modulation characteristics as the global positioning system (GPS) coarse/acquisition (C/A) signal. Due to its linearity and simplicity, BPSK is especially suitable for time-based positioning and a common choice in the PNT context [19]. Furthermore, besides their relevance, the choice of using basic PNT signals is motivated by the goal of not adding additional complexity to the receiver implementation, steering our attention to the proposed technique robustness in a baseline implementation. However, it is important to remark that, in principle, any heterogeneous set of known waveforms can be tracked through a VWB architecture, although one must carefully consider the resulting complexity burden during MC processing.

Two different satellite passages were analyzed to offer two different Doppler scenarios. A low elevation peak (LEP) passage with mild Doppler conditions and a lower average C/N_0; and a passage above the zenith, namely high elevation peak (HEP) passage, subject to intense Doppler conditions, a generally nonlinear Doppler profile, and a

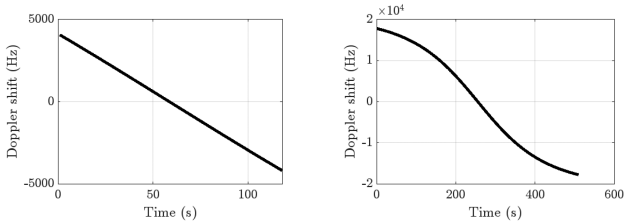

Fig. 6. Doppler shift for different satellite passages. (a) LEP passage. (b) HEP passage.

TABLE II
Scenario Characterization

Doppler profile	Average C/N_0 (dB-Hz)	Average power[a] (dBW)	Passage duration (s)
LEP	40.0	−158.0	117
HEP	50.0	−149.0	509

[a]Carrier isotropic power.

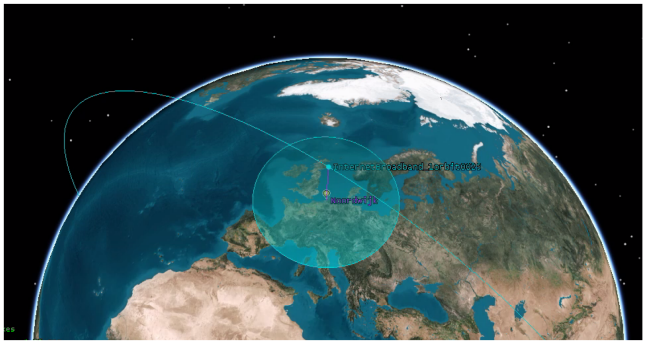

Fig. 7. Simulated scenario. High-elevation satellite passage example.

higher average C/N_0. The characteristics of these trajectories depend on the constellation configuration in Table I and each test is repeated for the two satellite passage profiles. The resulting Doppler frequency shifts along time are shown in Fig. 6 and the configurations for these two scenarios are reported in Table II.

A snapshot of the simulated scenario in the LEO constellation propagator software (AGI STK) is reported in Fig. 7. In the proposed frame, the satellite is at the zenith with respect to the user.

The main performance metric is the code estimation error, measured as the output of the DLL discriminator extracted within the receiver's tracking stage. This metric will be referred to as *discriminator output* and measured in chips. The two-step approach allows us to compare an SC output of a plain tracking stage (first step) with the result from MC processing (second step, Fig. 1). The performance can be then discussed by comparing the steady-state condition of the code estimation error in the two cases. The standard deviation (STD) of the discriminator output σ_d will be estimated (in meters) and used as an aggregated metric for ease of comparison among the experiments. The STD will be computed separately over the SC processing stage and the MC processing stage.

Notice that the MC triggering condition was forced to be activated only after a certain amount of time. This means that the condition of having the PLI value above the threshold is not considered until a certain number of tracking iterations (corresponding to 20 s). This allows the SC stage to last longer in order to provide sufficient data for statistical characterization of the discriminator output. Furthermore, a transient of about 1 s was noticed across all the tests. Consequently, an initial portion of 2 s is left out from the statistical analysis to accommodate the transient with some margin and avoid the latter causing degraded observations.

During the experiments, the output of the loop filter acting on the discriminator output (see Fig. 2) was monitored as well. This quantity, used to steer the code NCO, can be converted to a measure of the code rate and is susceptible to line of sight (LOS) dynamic stress, such as Doppler effects. To remove the Doppler dependency, we employed a quasi-noiseless signal—a LOS signal simulated at a very high C/N_0 of 100 dB-Hz adopted as a reference. The code rate estimate obtained in an SC tracking loop from this signal was subtracted from the MC code rate estimate under test. The resulting metric is reported to complement the performance analysis providing an accurate measure of the estimated *code-rate error*. This not only enables observation of the estimation error with respect to a ground truth reference but also allows the detection of biased estimation processes.

Indeed, as described in Section II-D, this metasignal approach introduces peak ambiguity in the ACF, potentially causing false-locking in the tracking, especially for signals impaired by MP. At each tracking loop iteration, the code rate estimate observed with the 100 dB-Hz LOS signal should differ with respect to what is measured with MP signals because of noise and possibly due to the presence of MP itself. However, on average, the difference in the two estimates, i.e. the code-rate error, should approach zero if the code rate estimation under MP is unbiased. Such monitoring of the estimation bias simulates the presence of a robust peak ambiguity resolution block, which could be implemented by resorting to well-established methods reported in the literature [49]. Although the outcomes of code-rate error averages are omitted for brevity, false locking monitoring was conducted for each set of experiments in Section IV, and no bias was detected. This successful validation of the two-step ambiguity resolution strategy carried out in specifically-designed challenging MP scenarios ensures the effectiveness of the approach under worst case conditions, as explained in the next section. The subsequent sections offer a more in-depth description of the study logic that guided the experiments for assessing the technique's performance (i)–(ii).

A. Performance Under Challenging MP Conditions

The MP tests are intended to challenge the receiver, inducing the conditions that are likely to trick the tracking stage to lock on a false locking point. The selected MP

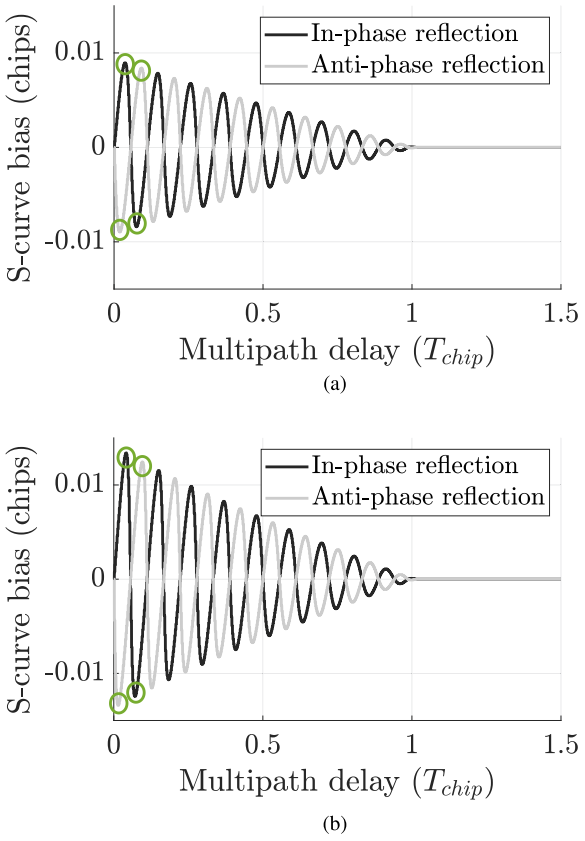

Fig. 8. MP errors induced by in-phase and antiphase reflection using a noncoherent E-L power normalized discriminator [24]. 2 BPSK(1) channels, virtual freq. separation 18.414 MHz, spacing = 0.025 chips. (a) Signal-to-multipath ratio (SMR) = 6 dB. (b) SMR = 3 dB.

TABLE III
Test-Dependent Settings

Test no.	Doppler profile	SMR (dB)	RS phase (rad)	RS delay (chips)
1	LEP	3	0	0.0418[a]
2	LEP	3	π	0.0141[b]
3	LEP	3	0	0.0717
4	LEP	3	π	0.0957
5	LEP	6	0	0.0365
6	LEP	6	π	0.019
7	LEP	6	0	0.0745
8	LEP	6	π	0.092
9	HEP	3	0	0.0418
10	HEP	3	π	0.0141
11	HEP	3	0	0.0717
12	HEP	3	π	0.0957
13	HEP	6	0	0.0365
14	HEP	6	π	0.019
15	HEP	6	0	0.0745
16	HEP	6	π	0.092
17	LEP	5–35	0–2π	0.002–0.512
18	HEP	5–35	0–2π	0.002–0.512

[a]Maximum S-curve bias.
[b]Minimum S-curve bias.

TABLE IV
Tested Receiver Configurations

Test no.	Doppler profile	DLL noise bandwidth (Hz)
1	LEP	150
2	LEP	250
3	HEP	150
4	HEP	250

model is a two-ray propagation model. The analysis is carried out using a specific narrow correlator (noncoherent E-L power normalized [55]), suitable for an effective false-lock mitigation. To this end, two different reflected signal (RS) amplitudes were selected, thus referring to as many diagrams, representing MP errors induced by in-phase and antiphase reflection, as shown in Fig. 8. Four different RS delays are ultimately selected for each of the plots, which are, therefore, "sampled" at the corresponding delays, choosing those values that are relevant for the locking robustness test. In particular, both for in-phase and antiphase RSs, the delays that give the maximum and minimum S-curve bias were selected (see the green circles in Fig. 8). The resulting values depend on the virtual frequency separation between channels (18.414 MHz), the type of discrimination function (noncoherent E-L power normalized [55]) and the discriminator spacing (0.025 chips). The RS is present for the full duration of the tests, that is, for both the SC and MC stages.

To complement the MP characterization, an additional set of experiments was performed under a realistic MP model (Tests 17 and 18). The simulated deterministic model was generated by modeling buildings and streets in a realistic urban scenario. At each instant, the position of the satellite and the user are considered, and the multiray propagation is computed based on the geometry and characteristics of the surfaces. The scattering model is based on radar cross-sections [56] while the ground reflections are simulated through Snell's law [57]. The resulting propagation environment is a multiray model with short-lifespan reflections in an urban scenario. Additionally, vehicular dynamics are simulated by specifying a user trajectory at constant speed. Table III summarizes the MP signal characteristics for each test.

B. Robustness With Respect to DLL Noise Bandwidth

The proposed VWB architecture was tested with respect to the amount of noise that the MC tracking loop can sustain. Two different Doppler profiles and C/N_0 levels were simulated as described by the LEP and HEP scenarios (see Table II). The MP configuration of Test 1 and Test 9 from Table III are selected to perform the tests in representative challenging MP conditions for, respectively, LEP and HEP scenarios. The aim is to stress the receiver within realistic conditions but varying the DLL noise bandwidth. Two different values of the DLL noise bandwidth were chosen arbitrarily, changing the previous working conditions of the DLL by increasing the loop bandwidth of up to one order of magnitude. The receiver configuration characteristics that drove the test campaign are summarized in Table IV.

TABLE V
STD of Discriminator Output Under Challenging MP Conditions

Test Id	1	2	3	4	5	6	7	8	17
SC estimated σ_d (m)	70.33	70.33	70.33	70.33	70.33	70.33	70.33	70.33	77.34
MC estimated σ_d (m)	5.57	5.57	5.57	5.57	5.57	5.57	5.57	5.57	5.33
σ_d reduction (%)	92.1	92.2	92.2	92.2	92.1	92.2	92.1	92.1	93.1

LEP satellite passage.

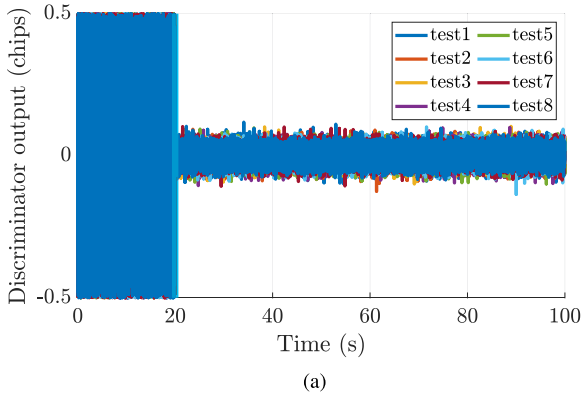

Fig. 9. Discriminator output of MP-affected signals. The cyan vertical line marks the beginning of the MC processing stage. Only the first 100 s are shown. (a) LEP satellite passage. (b) HEP satellite passage.

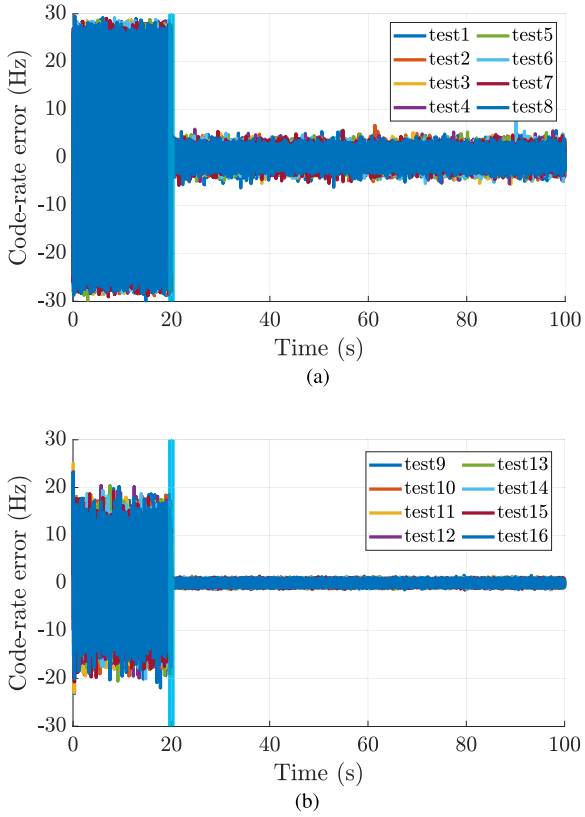

Fig. 10. Code-rate error of MP-affected signals. The cyan vertical line marks the beginning of the MC processing stage. Only the first 100 s are shown. (a) LEP satellite passage. (b) HEP satellite passage.

IV. RESULTS

In this section, we present the results of the experimental campaign. A comprehensive discussion on the investigation outcomes under different conditions is provided, according to the tested scenarios defined in Section III.

A. Performance Under Challenging MP Conditions

The examination of the DLL observables was performed for the two reference Doppler profiles scenarios of Fig. 6 (LEP and HEP). In each test, the signals are impaired by a different MP condition. However, each of the two satellite passages has a constant duration for the Earth-located user, favoring the aggregation of the test data by satellite passage scenario. Focusing on the LEP scenario, the time series of discriminator output and code-rate error are reported in Figs. 9(a) and 10(a), respectively, where the results from Tests 1 to 8 are superimposed. In the figure, a clear reduction of the code tracking noise is visible once the MC processing is activated (highlighted by the cyan vertical line).

At first glance, the outcomes of the tracking loops have the same behavior under all the different MP scenarios. This should come as no surprise since according to Fig. 8, the MP characteristics are almost equally challenging. The MP-induced errors cause, indeed, a set of *S*-curve bias values of the same order of magnitude for the selected RS configurations. The results of Fig. 9 have been aggregated for an easier comparison and reported in Table V. The STD of the discriminator output (σ_d) is computed both over the SC and the MC processing outcomes (first and second steps). Comparing the two sets of values, it is possible to observe that a less noisy discriminator output through SC processing corresponds to a low noise estimation through MC combining. The two sets have, therefore, similar trends. However, their magnitudes are much more different. In fact, as highlighted by the last row of Table V, the STD reduction

TABLE VI
STD of Discriminator Output Under Challenging MP Conditions

Test Id	9	10	11	12	13	14	15	16	18
SC estimated σ_d (m)	29.31	29.31	29.31	29.31	29.31	29.31	29.31	29.31	29.54
MC estimated σ_d (m)	1.76	1.76	1.76	1.76	1.76	1.76	1.76	1.76	2.67
σ_d reduction (%)	94.3	94.3	94.3	94.3	94.3	94.2	94.2	94.2	91.0

HEP satellite passage.

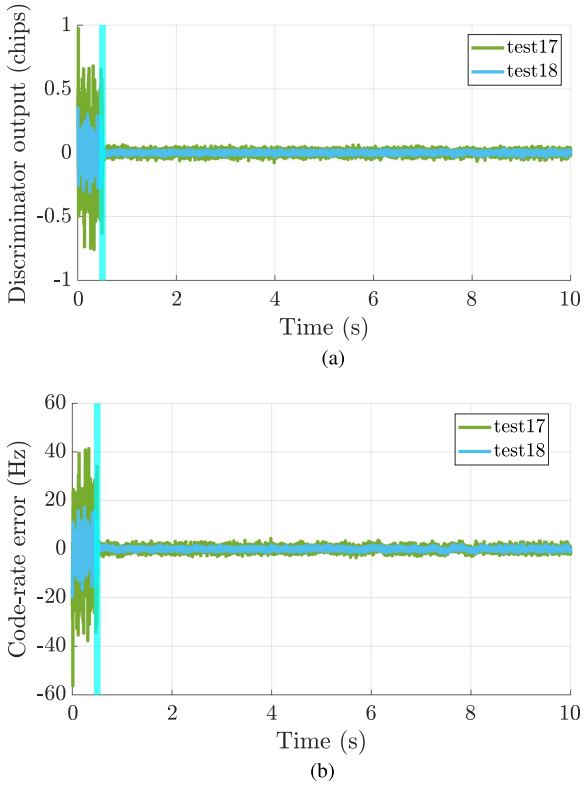

Fig. 11. DLL observables under the dynamic multiray model. LEP and HEP scenarios are superimposed. Due to the large computational burden, only 10 s were simulated and a 0.5 s delayed MC triggering was enforced. (a) Discriminator outputs. (b) Code-rate errors.

produced by the MC stage is always more than 90% for all the tests and σ_d is reduced by about one order of magnitude. The technique is, therefore, beneficial in this scenario under all the tested MP configurations.

The HEP scenario is characterized by higher Doppler levels and a nonlinear Doppler profile [see Fig. 6(b)]. However, the higher C/N_0 associated with the scenario should improve the estimation quality. Looking at the DLL metrics reported in Figs. 9(b) and 10(b), a reduction of the estimation noise is visible with respect to the LEP scenario. This result is also confirmed by the aggregated discriminator output data of Table VI.

The outcomes derived under the dynamic multiray model are depicted in Fig. 11. These resultant values align closely with the previously obtained results for the two-ray scenario, as also indicated in Tables V and VI. The observation of such comparable outcomes reaffirms the advantageous trait of a high-slope multipeaked ACF in managing close-in MP scenarios [46]. Additionally, this realistic setting emphasizes the presence of generally weaker reflected rays, which have a reduced ability to disrupt a locked tracking loop.

TABLE VII
STD of Discriminator Output

Doppler profile	LEP		HEP	
Test Id	Test 1	Test 2[a]	Test 3	Test 4
SC estimated σ_d (m)	79.12	82.05	41.03	64.47
MC estimated σ_d (m)	5.86	5.86	2.05	2.05
σ_d reduction (%)	92.3	92.5	95.0	96.8

Tests under extended DLL noise bandwidth
[a]DLL BW = 176 Hz .

Comparing Tables V and VI, it is clear that the higher C/N_0 of this last scenario dominates the performance with respect to the harsher Doppler conditions. A generally lower discriminator output noise is in fact visible both for the SC and the MC processing, where STD values move from about 29 m to less than 2 m. Nonetheless, the gain provided by the technique through σ_d reduction is comparable with the reduction in Table V. This shows that the effectiveness of the technique is not greater under such higher C/N_0 and nonlinear Doppler scenario but rather it acts on an already more accurate estimation.

B. Robustness With Respect to DLL Tracking Noise

The capability of the proposed architecture to mitigate signals affected by MP was further challenged in the following tests to assess the potential of the VWB tracking loop to bear noise within the DLL. A set of tests has been performed according to the study logic of Section III-B.

In the tested conditions, the VWB receiver can track a signal affected by MP using a DLL noise bandwidth as wide as 150 Hz. This was demonstrated in the first test of the LEP scenario (Test 1 from Table IV). Fig. 12(a) reports the result of the discriminator output. In the figure, the STD of the discriminator output moves from 79.12 m during the SC stage to 5.86 m for MC processing, resulting in an STD reduction of 92 %, as reported in Table VII.

The successful tracking for this test can be confirmed by looking at the code-rate error in Fig. 13(a) and the main observables estimated within the tracking stage, shown in Fig. 14(a). In the figure, the estimated Doppler carrier frequency matches the profile of the current scenario [see Fig. 6(a)], the code-rate estimate (lower plot) is consistent with the profile as well and positioned around the correct

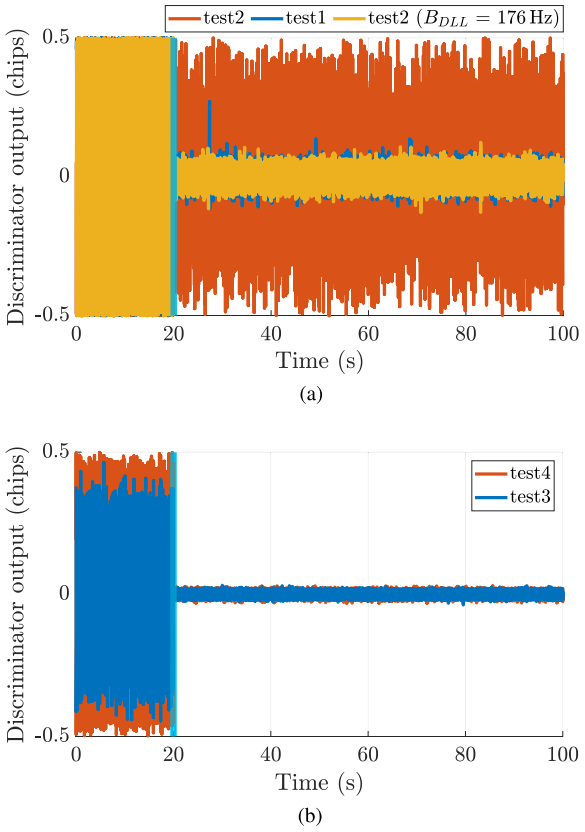

Fig. 12. Discriminator output of MP-affected signals using different DLL noise bandwidths. Only the first 100 s are shown. (a) LEP satellite passage. (b) HEP satellite passage.

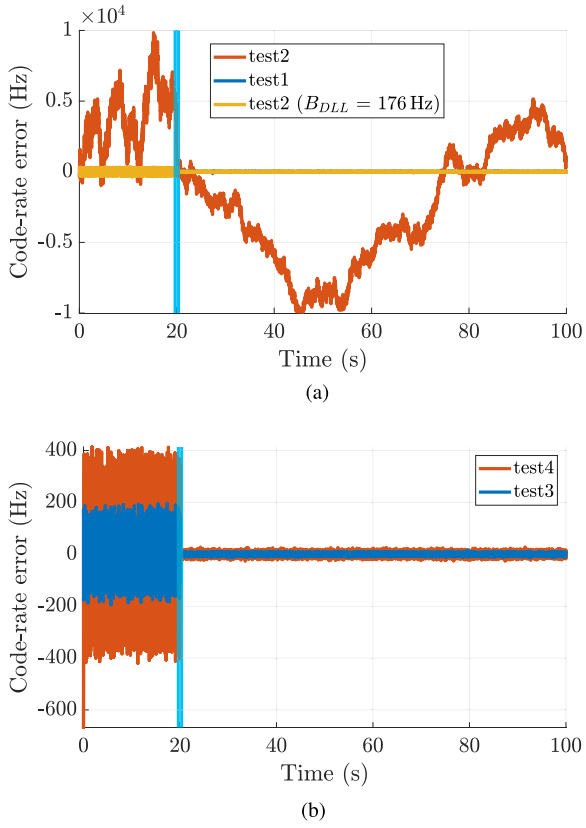

Fig. 13. Code-rate error of MP-affected signals using different DLL noise bandwidths. Only the first 100 s are shown. (a) LEP satellite passage. (b) HEP satellite passage.

values, and the values of I_P and Q_P (top plot) are correctly separated, evidence of phase locking.

On the other hand, the same signal received using a 250-Hz DLL bandwidth as for Test 2 in Table IV cannot be tracked. This is clearly visible by inspecting the code-rate error in Fig. 13(a) and the outcome of the tracking stage in Fig. 14(b), where the estimates are completely off-target and the I_P and Q_P components are continuously mixed. It is worth stressing, however, that setting such a large DLL bandwidth disrupts the performance of the plain SC receiver as well, as shown in the first 20 s of the plots in Figs. 13(a) and 14(b). The latter shows, indeed, a similar behavior and it cannot track the incoming signal.

In the current scenario, the maximum DLL bandwidth that allows us to successfully track the incoming signal is 176 Hz. The discriminator output and code-rate error in this configuration are also reported in Figs. 12(a) and 13(a) and the advantage provided by the technique by means of STD reduction is shown again in Table VII, where the discriminator output is reduced from around 82 m to 5.86 m.

A plain SC receiver under the same conditions can tolerate a DLL bandwidth of up to 220 Hz, as shown by Fig. 14(c). An MC DLL block is, thus, less robust to noise with respect to a plain DLL. However, a 176-Hz bandwidth is much higher than what is necessary to successfully track signals in the investigated scenarios (20 Hz was set for other experiments, see Table I); therefore, it can potentially enable also the tracking of signals transmitted at higher carrier frequencies.

The higher C/N_0 of the HEP scenario is again less challenging for the MC receiver, despite the nonlinear Doppler profile of the scenario. The more favorable C/N_0 allows the VWB receiver to successfully track the signal during both HEP tests (Test 3 and Test 4), bearing a DLL bandwidth, which can be as wide as 250 Hz. The benefits provided by the MC tracking in such conditions are visible in Figs. 12(b) and 13(b) and summarized in Table VII through the observation of σ_d. It is interesting to notice that the difference between the SC estimated σ_d of the two tests is larger than the LEP case. The SC estimated σ_d experienced for a reduced DLL bandwidth (Test 3) is smaller than what was experienced in Test 4. However, the use of MC tracking is more effective for Test 4, resulting in two comparable performances when it is activated.

V. CONCLUSION

In this document, a deep characterization of the VWB receiver and its performance in a LEO PNT scenario has been provided. The outcomes from these investigations allow us to draw several important conclusions that are addressed in the following.

The analysis of the performance under challenging MP conditions of Section IV-A demonstrated that the technique can cope with the MP impairment in a simplified two-ray

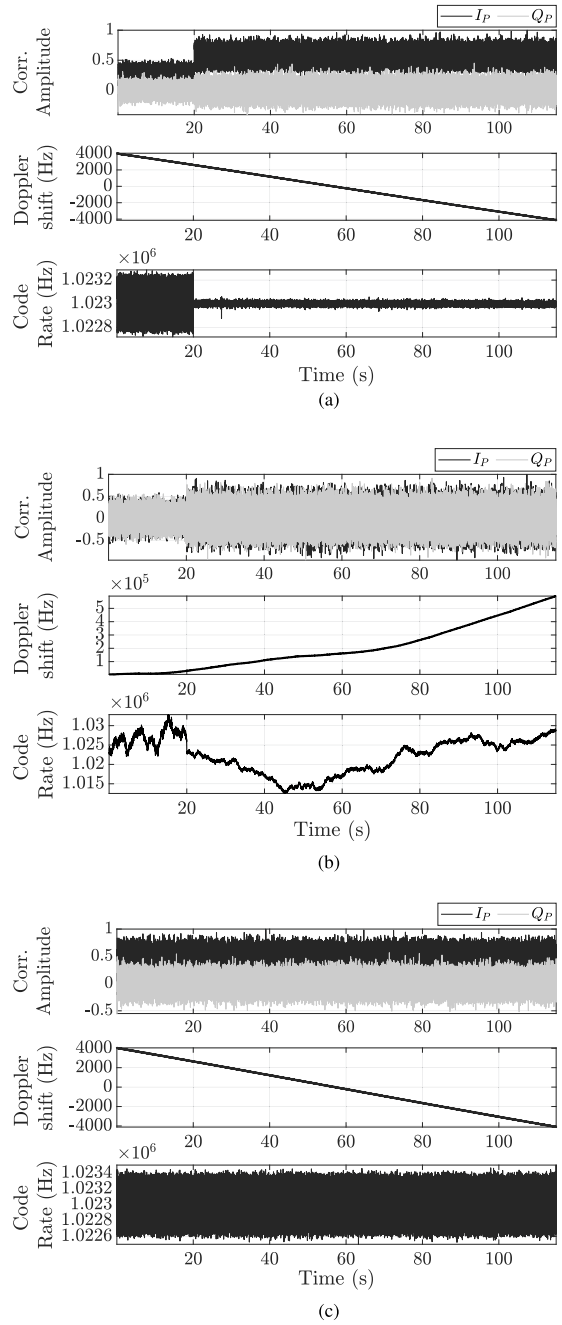

Fig. 14. Tracking loop observables for different DLL bandwidths. LEP scenario. (a) Test 1 (DLL bandwidth = 150 Hz). (b) Test 2 (DLL bandwidth = 250 Hz). (c) Test 2 (DLL bandwidth = 220 Hz). SC receiver.

scenario. The tests performed showed a very similar response to different RS delays and amplitudes (see Tables V and VI). Moreover, despite different C/N_0 and Doppler conditions, a similar performance gain could be observed, with σ_d reduction that is always above 90%. The technique is, therefore, beneficial in a LEO PNT framework and in a scenario characterized by signals affected by moderate MP (e.g., some urban or suburban scenarios). In particular, the analysis of the HEP scenario highlighted how a higher C/N_0 is more desirable than a less-challenging Doppler profile. Thanks to the use of a narrowband approach, the proposed architecture reacts well under challenging Doppler conditions. As a result, C/N_0 is the dominant performance driver with respect to the Doppler shift.

To test the MC DLL response to noise, a loop bandwidth extension has been tested in Section IV-B. For a relevant extension to 150 Hz, a moderate performance worsening has been observed with respect to the MP tests. To this purpose, compare Test 1 and Test 9 from Tables V and VI with Test 1 and Test 3 from Table VII, respectively. This means that the receiver can likely track higher Doppler rates, without disrupting its code estimation accuracy. It has been also observed, however, that the proposed architecture is less robust to noise than a plain SC receiver. The latter is in fact able to track a signal received at 40 dB-Hz, within the LEP scenario, using a DLL bandwidth of 220 Hz. On the other hand, a VWB receiver can correctly track the same signal using a loop as large as 176 Hz, whereas a larger bandwidth would let the noise disrupt the tracking. Nevertheless, a 176-Hz bandwidth is a reasonable range, even for the challenging LEO PNT scenario under consideration. Furthermore, with a higher C/N_0 level, such as that in the HEP scenario, the VWB can correctly track a signal received with a 250-Hz loop bandwidth, with a minimal performance loss with respect to a 20-Hz bandwidth (compare Test 9 of Table VI with Test 4 of Table VII). This is quite reasonable since the harsher Doppler conditions of the HEP scenario are well tolerated by the extended loop bandwidth while the better C/N_0 ratio helps in reducing the amount of noise that enters the loop through the widened noise bandwidth.

These results provide an insightful characterization of this MC technique, which has been proven adequate to successfully follow the representative Doppler profiles and C/N_0 levels of the addressed LEO PNT scenario, under moderate MP conditions. The VWB architecture has the potential to be beneficial in the LEO PNT paradigm, at the cost of a larger complexity on the user side. Nevertheless, during the design process of the LEO PNT system, performance improvement could be obtained also in other ways, acting at the signal level, thus balancing the increased complexity between system and user side.

ACKNOWLEDGMENT

The project was carried out in the scope of investigating "Enhanced GNSS signals in space and user receiver processing" in response to ESA AO-1-9585/19/NL/CRS, Activity No. 1000023741 in the "esa-star" system, Item no. 18.1ET.29.

REFERENCES

[1] European Union Agency for the Space Program, "EUSPA EO and GNSS market report," Prague, Czech Republic, Tech. Rep., 2022, doi: 10.2878/94903.

[2] W. Wang, N. Okati, I. Tanash, T. Riihonen, and E.-S. Lohan, "Location-based beamforming architecture for efficient farming applications with drones," in *Proc. Int. Conf. Localization GNSS*, 2019, pp. 1–6.

[3] A. Minetto, A. Nardin, and F. Dovis, "Tight integration of GNSS measurements and GNSS-based collaborative virtual ranging," in *Proc. 31st Int. Tech. Meeting Satell. Division Inst. Navigation*, 2018, pp. 2399–2413.

[4] A. Minetto, A. Nardin, and F. Dovis, "GNSS-only collaborative positioning among connected vehicles," in *Proc. 1st ACM MobiHoc Workshop Technol., Models, Protoc. Cooperative Connected Cars*, 2019, pp. 37–42, doi: 10.1145/3331054.3331552.

[5] A. Minetto, A. Nardin, and F. Dovis, "Modelling and experimental assessment of inter-personal distancing based on shared GNSS observables," *Sensors*, vol. 21, no. 8, pp. 1–26, 2021. [Online]. Available: https://www.mdpi.com/1424-8220/21/8/2588

[6] M. Pini et al., "Satellite-derived time for enhanced telecom networks synchronization: The root project," in *Proc. IEEE 8th Int. Workshop Metrol. AeroSpace*, 2021, pp. 288–293.

[7] A. Minetto, F. Dovis, A. Nardin, O. Vouch, G. Impresario, and M. Musmeci, "Analysis of GNSS data at the Moon for the LuGRE project," in *Proc. IEEE 9th Int. Workshop Metrol. AeroSpace*, 2022, pp. 134–139.

[8] A. Nardin, A. Minetto, O. Vouch, M. Maiani, and F. Dovis, "Snapshot acquisition of GNSS signals in space: A case study at lunar distances," in *Proc. 35th Int. Tech. Meeting Satell. Division Inst. Navigation*, 2022, pp. 3603–3617.

[9] A. Nardin, A. Minetto, S. Guzzi, F. Dovis, L. Konitzer, and J. J. K. Parker, "Snapshot tracking of GNSS signals in space: A case study at lunar distances," in *Proc. 36th Int. Tech. Meeting Satell. Division Inst. Navigation*, 2023, pp. 3267–3281.

[10] R. Hirokawa, I. Fernández-Hernández, and S. Reynolds, "PPP/PPP-RTK open formats: Overview, comparison, and proposal for an interoperable message," *NAVIGATION: J. Inst. Navigation*, vol. 68, no. 4, pp. 759–778, 2021. [Online]. Available: https://navi.ion.org/content/68/4/759

[11] X. Zhang, Z. Yao, and M. Lu, "Optimizing the Gabor bandwidth of satellite navigation signals by MCS signal expression," *Sci. China Phys. Mechanics Astron.*, vol. 54, no. 6, pp. 1077–1082, Jun. 2011.

[12] A. Emmanuele, M. Luise, F. Zanier, and M. Crisci, "Selective accuracy and multiresolution capabilities are intrinsic features of multicarrier waveforms for GNSS," in *Proc. 6th ESA Workshop Satell. Navigation Technol., Eur. Workshop GNSS Signals Signal Process.*, 2012, pp. 1–8.

[13] P. Dabove and V. Di, "Pietra towards high accuracy GNSS real-time positioning with smartphones," *Adv. Space Res.*, vol. 63, no. 1, pp. 94–102, 2019. [Online]. Available: https://www.sciencedirect.com/science/article/pii/S0273117718306537

[14] A. Nardin, F. Dovis, and J. A. Fraire, "Empowering the tracking performance of LEO-based positioning by means of meta-signals," *IEEE J. Radio Freq. Identif.*, vol. 5, no. 3, pp. 244–253, Sep. 2021.

[15] Z. Yao, J. Ma, J. Zhang, and M. Lu, "Multicarrier constant envelope composite signal - A solution to the next generation satellite navigation signals," in *Proc. 30th Int. Tech. Meeting Satell. Division Inst. Navigation*, 2017, pp. 1520–1533. [Online]. Available: https://www.ion.org/publications/abstract.cfm?articleID=15372

[16] Z. Yao, F. Guo, J. Ma, and M. Lu, "Orthogonality-based generalized multicarrier constant envelope multiplexing for DSSS signals," *IEEE Trans. Aerosp. Electron. Syst.*, vol. 53, no. 4, pp. 1685–1698, Aug. 2017. [Online]. Available: https://ieeexplore.ieee.org/document/7858582/

[17] P. Teunissen and O. Montenbruck, *Springer Handbook of Global Navigation Satellite Systems*. Berlin, Germany: Springer, 2017.

[18] R. Knight, "ESA outlines plans for demo of LEO PNT satellites as part of FutureNAV, gives other updates," *Inside GNSS*, 2022. Accessed: Dec. 31, 2022. [Online]. Available: https://insidegnss.com/esa-outlines-plans-for-demo-of-leo-pnt-satellites-as-part-of-futurenav-gives-other-updates/

[19] F. S. Prol et al., "Position, navigation, and timing (PNT) through low earth orbit (LEO) satellites: A survey on current status, challenges, and opportunities," *IEEE Access*, vol. 10, pp. 83971–84002, 2022.

[20] T. G. Reid et al., "Satellite navigation for the age of autonomy," in *Proc. IEEE/ION Position, Location, Navigation Symp.*, 2020, pp. 342–352. [Online]. Available: https://ieeexplore.ieee.org/document/9109938/

[21] F. van Diggelen, "High-sensitivity GNSS," in *Position, Navigation, and Timing Technologies in the 21st Century*. Hoboken, NJ, USA: Wiley, 2020, pp. 445–479. [Online]. Available: http://onlinelibrary.wiley.com/doi/abs/10.1002/9781119458449.ch18

[22] A. Nardin, F. Dovis, and J. A. Fraire, "Empowering the tracking performance of LEO PNT by means of meta-signals," in *Proc. IEEE Int. Conf. Wireless Space Extreme Environ.*, 2020, pp. 153–158.

[23] Z. Yao and M. Lu, *Next-Generation GNSS Signal Design*. Singapore:Springer, 2021.

[24] E. Kaplan and C. Hegarty, *Understanding GPS/GNSS: Principles and Applications*. Norwood, MA, USA: Artech House, 2017.

[25] C. Wang, X. Cui, T. Ma, S. Zhao, and M. Lu, "Asymmetric dual-band tracking technique for optimal joint processing of BDS B1I and B1C signals," *Sensors*, vol. 17, no. 10, Oct. 2017, Art. no. 2360. [Online]. Available: https://www.mdpi.com/1424-8220/17/10/2360

[26] W. Zhang, Z. Yao, and M. Lu, "WHAT: Wideband high-accuracy joint tracking technique for BDS B1 composite signal," in *Proc. IEEE 9th Int. Conf. Electron. Inf. Emerg. Commun.*, 2019, pp. 178–182.

[27] Y. Gao, Z. Yao, and M. Lu, "High-precision unambiguous tracking technique for BDS B1 wideband composite signal," *Navigation*, vol. 67, no. 3, pp. 633–650, 2020. [Online]. Available: https://onlinelibrary.wiley.com/doi/abs/10.1002/navi.377

[28] Z. Tian, X. Cui, G. Liu, and M. Lu, "LPRA-DBT: Low-processing-rate asymmetrical dual-band tracking method for BDS-3 B1I and B1C composite signal," in *Proc. Int. Tech. Meeting Inst. Navigation*, 2022, pp. 1027–1038.

[29] C. Wang, X. Cui, T. Ma, S. Zhao, and M. Lu, "Asymmetric dual-band tracking technique for optimal joint processing of BDS B1I and B1C signals," *Sensors*, vol. 17, no. 10, pp. 1–16, 2017. [Online]. Available: https://www.mdpi.com/1424-8220/17/10/2360

[30] J.-L. Issler, M. Paonni, and B. Eissfeller, "Toward centimetric positioning thanks to L-and S-band GNSS and to meta-GNSS signals," in *Proc. 5th ESA Workshop Satell. Navigation Technol. Eur. Workshop GNSS Signals Signal Process.*, 2010, pp. 1–8.

[31] M. Paonni, J. Curran, M. Bavaro, and J. Fortuny, "GNSS meta-signals: Coherently composite processing of multiple GNSS signals," in *Proc. 27th Int. Tech. Meeting Satell. Division Inst. Navigation*, 2014, pp. 8–12.

[32] P. Das, L. Ortega, J. Vilà-Valls, F. Vincent, E. Chaumette, and L. Davain, "Performance limits of GNSS code-based precise positioning: GPS, Galileo & meta-signals," *Sensors*, vol. 20, no. 8, pp. 1–32, 2020. [Online]. Available: https://www.mdpi.com/1424-8220/20/8/2196

[33] L. Ortega, D. Medina, J. Vilà-Valls, F. Vincent, and E. Chaumette, "Positioning performance limits of GNSS meta-signals and HO-BOC signals," *Sensors*, vol. 20, no. 12, Jun. 2020, Art. no. 3586. [Online]. Available: https://www.mdpi.com/1424-8220/20/12/3586

[34] D. Borio and C. Gioia, "Reconstructing GNSS meta-signal observations using sideband measurements," *NAVIGATION: J. Inst. Navigation*, vol. 70, no. 1, 2023. [Online]. Available: https://navi.ion.org/content/70/1/navi.558

[35] D. Borio, "Hypercomplex representation and processing of GNSS signals," in *Proc. 35th Int. Tech. Meeting Satell. Division Inst. Navigation*, 2022, pp. 3160–3179.

[36] M. S. Hameed, T. Woerz, T. Pany, J. Wendel, M. Paonni, and T. Senni, "Demonstration of meta-signal positioning using LAMBDA ambiguity fixing method within a bit-true simulation," in *Proc. 34th Int. Tech. Meeting Satell. Division Inst. Navigation*, 2021, pp. 2819–2837.

[37] J. Garcia-Molina, "Unambiguous meta-signal processing: A path to code-based high-accuracy PNT," *Inside GNSS*, vol. 16, no. 2, pp. 50–55, Mar. 2021.

[38] C. Schwalm, C. Enneking, and S. Thoelert, "Ziv-Zakai bound and multicorrelator compression for a Galileo E1 meta-signal," in *Proc. Eur. Navigation Conf.*, 2020, pp. 1–9.
[39] European Union, "European GNSS (Galileo) open service, signal-in-space interface control document (OS SIS ICD V2.0)," Jan. 2021. [Online]. Available: https://www.gsc-europa.eu/sites/default/files/sites/all/files/Galileo_OS_SIS_ICD_v2.0.pdf
[40] T. Reid, "Opportunities in commercial LEO satellite navigation," in *Proc. 34th Int. Tech. Meeting Satell. Division Inst. Navigation*, 2021, pp. 2012–2048. [Online]. Available: http://www.ion.org/publications/abstract.cfm?jp=p&articleID=18106
[41] P. A. Iannucci and T. E. Humphreys, "Economical fused LEO GNSS," in *Proc. IEEE/ION Position, Location, Navigation Symp.*, 2020, pp. 426–443.
[42] A. Nardin, F. Dovis, and B. Motella, "Impact of non-idealities on GNSS meta-signals processing," in *Proc. Eur. Navigation Conf.*, 2020, pp. 1–8.
[43] R. McDonough and A. Whalen, *Detection of Signals in Noise*. Amsterdam, The Netherlands: Elsevier, 1995, pp. 383–445.
[44] J. W. Betz and K. R. Kolodziejski, "Generalized theory of code tracking with an early-late discriminator Part I: Lower bound and coherent processing," *IEEE Trans. Aerosp. Electron. Syst.*, vol. 45, no. 4, pp. 1538–1556, Oct. 2009. [Online]. Available: https://ieeexplore.ieee.org/document/5310316/
[45] J. W. Betz, "The offset carrier modulation for GPS modernization," in *Proc. Nat. Tech. Meeting Inst. Navigation*, 1999, pp. 639–648.
[46] A. Nardin, "Innovative signal processing solutions for next-generation satellite navigation systems," Ph.D. dissertation, Dept. Electron. Telecommun. (DET), Politecnico di Torino, Torino, Italy, 2023.
[47] A. Weiss and E. Weinstein, "Fundamental limitations in passive time delay estimation—Part I: Narrow-band systems," *IEEE Trans. Acoust., Speech, Signal Process.*, vol. ASSP-31, no. 2, pp. 472–486, Apr. 1983.
[48] E. Weinstein and A. Weiss, "Fundamental limitations in passive time-delay estimation—Part II: Wide-band systems," *IEEE Trans. Acoust., Speech, Signal Process.*, vol. ASSP-32, no. 5, pp. 1064–1078, Oct. 1984.
[49] J. Wendel, F. M. Schubert, and S. Hager, "A robust technique for unambiguous BOC tracking," *NAVIGATION*, vol. 61, no. 3, pp. 179–190, 2014.
[50] Z. Yao, Y. Gao, Y. Gao, and M. Lu, "Generalized theory of BOC signal unambiguous tracking with two-dimensional loops," *IEEE Trans. Aerosp. Electron. Syst.*, vol. 53, no. 6, pp. 3056–3069, Dec. 2017.
[51] J. J. Spilker Jr., P. Axelrad, B. W. Parkinson, and P. Enge, *Global Positioning System: Theory and Applications, Volume I*. Amer. Inst. Aeronaut. Astronaut., Washington, DC, USA, 1996.
[52] Z. M. Kassas et al., "Navigation with multi-constellation LEO satellite signals of opportunity: Starlink, OneWeb, Orbcomm, and Iridium," in *Proc. IEEE/ION Position, Location, Navigation Symp.*, 2023, pp. 338–343.
[53] M. Su, X. Su, Q. Zhao, and J. Liu, "BeiDou augmented navigation from low earth orbit satellites," *Sensors*, vol. 19, no. 1, pp. 1–17, 2019. [Online]. Available: https://www.mdpi.com/1424-8220/19/1/198
[54] I. del Portillo, B. G. Cameron, and E. F. Crawley, "A technical comparison of three low earth orbit satellite constellation systems to provide global broadband," *Acta Astronautica*, vol. 159, pp. 123–135, 2019. [Online]. Available: https://www.sciencedirect.com/science/article/pii/S0094576518320368
[55] E. Kaplan and C. Hegarty, *Understanding GPS: Principles and Applications*. Norwood, MA, USA: Artech House, 2005.
[56] B. Chen and C. Tong, "Radar multipath scattering from the composite model: Specular image modified model and ISAR imaging analysis," *Int. J. RF Microw. Comput.-Aided Eng.*, vol. 29, no. 12, 2019, Art. no. e21956. [Online]. Available: https://onlinelibrary.wiley.com/doi/abs/10.1002/mmce.21956
[57] R. U. R. Lighari, M. Berg, J. Kallankari, A. Parssinen, and E. T. Salonen, "Analysis of the measured RHCP and LHCP GNSS signals in multipath environment," in *Proc. Int. Conf. Localization GNSS*, 2016, pp. 1–6.

Andrea Nardin (Graduate Student Member, IEEE) received the M.Sc. degree in telecommunications engineering and the Ph.D. degree in electrical, electronics, and communications engineering from Politecnico di Torino, Turin, Italy, in 2018 and 2023, respectively.

He is currently a Postdoctoral Researcher with the Department of Electronics and Telecommunications, Politecnico di Torino. Since 2018, he has been with the Navigation Signal Analysis and Simulation (NavSAS) group, Politecnico di Torino. In 2021, he was a Visiting Doctoral Researcher with Northeastern University, Boston, MA, USA, with the Center for Signal Processing, Imaging, Reasoning, and Learning (SPIRAL). His research interests include signal processing architectures and signal design applied to GNSSs and LEO PNT.

Fabio Dovis (Member, IEEE) was born in Bruino, Italy, in 1970. He received the M.Sc. in electronics engineering and the Ph.D. degree in electronics and communications engineering from Politecnico di Torino, Turin, Italy, in 1996 and 2000, respectively.

He joined the Department of Electronics and Telecommunications, Politecnico di Torino, as an Assistant Professor in 2004 and as Associate Professor in 2014. Since 2021, he has been a Full Professor with the same department where he coordinates the Navigation Signal Analysis and Simulation (NavSAS) research group. He has a relevant experience in European projects in satellite navigation as well as cooperation with industries and research institutions. His research interests include the design of GPS and Galileo receivers and advanced signal processing for interference and multipath detection and mitigation, as well as ionospheric monitoring.

Dr. Dovis is a member of the IEEE Aerospace and Electronics Systems Society Navigation Systems Panel.

Francesca Zanier received the M.Sc. degree in telecommunications engineering and the Ph.D. degree in information engineering from the University of Pisa, Pisa, Italy, in 2009.

In 2009, she joined European Space Agency, ESTEC, Noordwijk, The Netherlands, where she is currently a Radio Navigation System Engineer with the Radio Navigation Systems and Techniques Section of the Technical Directorate. Her research interests include signal processing, estimation theory, GNSS receivers, and signals and navigation applications.

Floor Melman received the master's degree in aerospace engineering from the Delft University of Technology (TU Delft), Delft, The Netherlands, in 2018.

From 2018 to 2020, he was a Young Graduate Trainee in the navigation directorate on Galileo signals and receivers. Since 2020, he has been a Radio Navigation Engineer with ESA/ESTEC. His main research interests include PNT algorithms (in harsh environments) and GNSS signal processing.

Open Access funding provided by 'Politecnico di Torino' within the CRUI CARE Agreement